Advances in Technology Innovation, vol. 10, no. 2, 2025, pp. 157-173

Formulating Seismic Intensity Scale (JMA-SIS) Using Response Spectrum: A New Approach for Structural Engineering Design

Nanang Gunawan Wariyatno[1,*], Ay Lie Han[2], Yanuar Haryanto[1,3,4], Gathot Heri Sudibyo[1], Sumiyanto[1], Nastain[1], Arwan Apriyono[1], Laurencius Nugroho[4], Hsuan-Teh Hu[4], Fu-Pei Hsiao[3], Buntara Sthenly Gan[5]

[1]Department of Civil Engineering, Universitas Jenderal Soedirman, Purwokerto, Indonesia

[2]Department of Civil Engineering, Universitas Diponegoro, Semarang, Indonesia

[3]National Center for Research on Earthquake Engineering, Taipei, Taiwan

[4]Department of Civil Engineering, National Cheng Kung University, Tainan, Taiwan

[5]Department of Architecture, Nihon University, Koriyama, Japan

Received 03 September 2024; received in revised form 10 December 2024; accepted 12 December 2024

DOI: https://doi.org/10.46604/aiti.2024.14243

Abstract

This study aims to formulate a calculation for earthquake shaking intensity (rs_mSIS) based on the response spectrum (RS) using the Japan Meteorological Agency-seismic intensity scale. The research investigates the relationship between the response spectrum parameters—period and maximum acceleration—and the earthquake source types, including megathrust, Benioff, and shallow crust/background sources. Artificial ground motions are generated and analyzed using Matlab to calculate shaking intensity values, which are then used to develop the rs_mSIS formula. The formulation is validated against actual response spectrum data from 15 Indonesian cities and demonstrated high accuracy, with the Wariyatno coefficient applicable across all models. This approach provides a standardized method to assess seismic intensity, offering enhanced reliability for building design in earthquake-prone areas and serving as a valuable tool for engineers and urban planners to improve earthquake resilience in diverse seismic environments.

Keywords: Japan Meteorological Agency-seismic intensity scale (JMA-SIS), time history, response spectrum, rs_mSIS, Wariyatno coefficient

1. Introduction

An earthquake is a natural geological event characterized by the sudden release of energy in the Earth's crust, resulting in seismic waves. This energy release typically occurs due to the displacement of tectonic plates along faults or fractures in the Earth's surface. Seismic waves originate in the bedrock and travel to the surface, passing through various soil layers. The intensity of ground shaking is influenced significantly by factors such as earthquake magnitude, distance from the epicenter, and soil composition, which affects how vibrations propagate [1]. Typically, earthquake shaking intensity decreases as the distance from the epicenter increases. [2]. For instance, the 2011 Tohoku earthquake, with a magnitude of 9, produced a maximum shaking intensity of 6.6 [3]. Such intensity measurements are crucial, as they provide valuable data for assessing structural impacts and guiding building design in seismic regions. Fig. 1 illustrates the distribution of maximum shaking intensity relative to the distance from the hypocenter during this earthquake.

Standards for measuring the earthquake shaking intensity on the ground surface include modified Mercalli intensity (MMI), Chinese seismic intensity scale (CSIS), European macroseismic scale (EMS), and environmental seismic intensity

* Corresponding author. E-mail address: nanang.wariyatno@unsoed.ac.id

English language proofreader: Si-Yu Lin

(ESI) [4-5]. In this research, the Japan Meteorological Agency-seismic intensity scale (JMA-SIS) [6-7], developed by the Japan Meteorological Agency (JMA), is utilized to categorize the intensity of local ground shaking caused by earthquakes. JMA-SIS quantifies ground shaking at measurement sites in affected areas, assigning levels from one to seven, with additional "strong" and "weak" subdivisions between levels five and six. This scale plays a critical role in Japan's disaster mitigation efforts, facilitating immediate and informative earthquake warnings broadcast nationally, which allows people to assess shaking severity in real-time. As shown in Fig. A1 (Appendix 1), JMA-SIS indicates that shaking at level 5^{Lower} may cause interior objects to fall, while structural damage to buildings potentially begins at level 6^{Lower} [8-9]. This standardized intensity scale enhances public safety by effectively communicating earthquake severity to the public and aiding in immediate response planning.

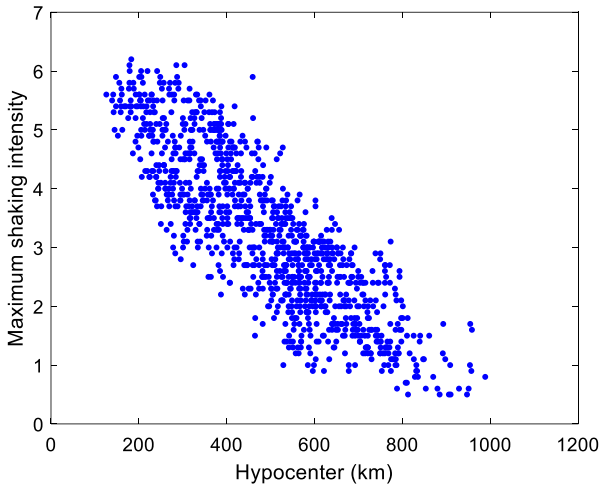

Fig. 1 The distribution of JMA_mSIS versus hypocenter in the Tohoku earthquake

The JMA-SIS level is determined based on the maximum-SIS (mSIS) values measured at the ground surface. These mSIS values are derived from ground motion acceleration data recorded in three directions: north-south (NS), east-west (EW), and up-down (UD) [10]. The lowest JMA-SIS level corresponds to an mSIS value of ≤ 0.5, while the highest level corresponds to an mSIS value of ≥ 6.5, as shown in Table 1 [11].

Table 1 Interval level JMA-SIS

No.	SIS	mSIS Interval
1	0	mSIS < 0.5
2	1	0.5 ≤ mSIS < 1.5
3	2	1.5 ≤ mSIS < 2.5
4	3	2.5 ≤ mSIS < 3.5
5	4	3.5 ≤ mSIS < 4.5
6	5^{Lower}	4.5 ≤ mSIS < 5.0
7	5^{Upper}	5.0 ≤ mSIS < 5.5
8	6^{Lower}	5.5 ≤ mSIS < 6.0
9	6^{Upper}	6.0 ≤ mSIS < 6.5
10	7	6.5 ≤ mSIS

The intensity of earthquake shaking significantly affects building damage and human casualties [12]. Specifically, higher shaking intensity correlates with an increased frequency of building failures, leading to a greater number of casualties. Data from the JMA (1996–2018) indicate that both fatalities and building damage increase as maximum shaking intensity (JMA_mSIS) levels rise [11]. The relationship between JMA_mSIS, fatalities, and building damage is illustrated in Fig. 2.

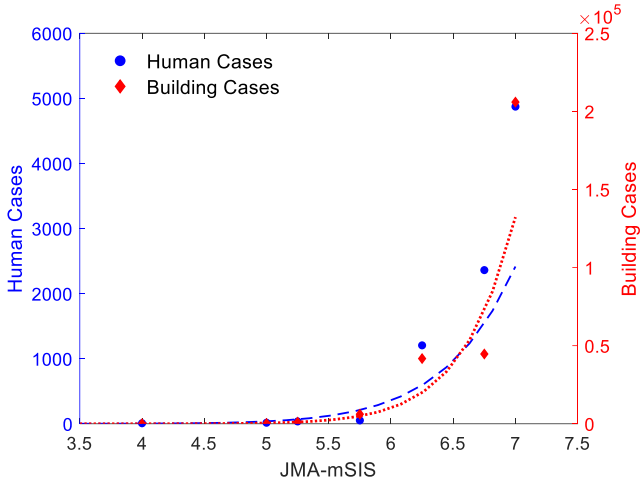

Fig. 2 Relationship between seismic intensity level and cases of human casualties and building damage

Each earthquake-induced ground motion has a unique shaking intensity and corresponding response spectrum (RS) [13-14]. The RS represents the maximum response of a single-degree-of-freedom (SDOF) structure to earthquake ground motion [15] and serves as a primary parameter in earthquake-resistant building design [16]. This spectrum is influenced by factors such as soil type and building location. In time history analysis, the applied load is an artificial ground motion generated through spectral matching or spectrum scaling to align with the target response spectrum [17]. The intensity of artificial ground motion can be assessed using the JMA_mSIS formula. This supports the hypothesis that a strong relationship exists between shaking intensity and response spectrum. In this study, earthquake shaking intensity is calculated using a response spectrum–based metric called rs_mSIS. Fig. 3 illustrates the relationship between shaking intensity and RS.

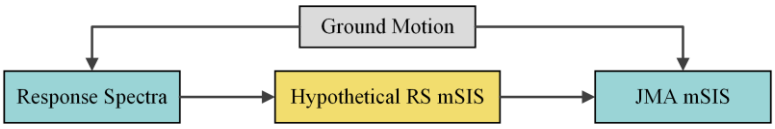

Fig. 3 Illustration of the relationship between mSIS and RS

This study aims to formulate the JMA-SIS using RS analysis, providing a predictive formula for seismic intensity based on a predetermined RS, improving the accuracy and comprehensibility of the intensity. Importantly, this approach does not change the design results for structures but instead offers a clearer interpretation of the earthquake intensity, which is crucial for public awareness. By employing RS analysis to determine seismic intensity, this study seeks to offer a tool that is easier to understand for both professionals and the general public when assessing earthquake risks to infrastructure. The JMA-SIS will help improve the understanding of structural resilience against seismic events, ultimately contributing to enhanced earthquake preparedness and more resilient infrastructure in earthquake-prone regions.

2. Methods

The complete research flowchart is shown in Fig. 4. This study uses both RS and ground motion data, each comprising model and validation datasets. The RS model data varied based on *Ts* (X-axis) and Sa_{max} (Y-axis) values, while the ground motion data are determined by the earthquake's mechanism, magnitude, and distance from the epicenter.

For each earthquake mechanism type, three sample ground motions are selected to represent all possible mechanisms. Artificial ground motions are generated using spectral matching with SeismoMatch software [18]. Before spectral matching, the ground motions are scaled to match the target RS for each direction [19]. The target RS used has a Sa_{max} value of 0.01 g for all *Ts* values. The artificial ground motions produced by spectral matching are then analyzed using the JMA-SIS program to calculate mSIS values for each RS variation. To vary the RS with respect to the Sa_{max} value [20], the artificial ground motions are scaled using a scaling factor based on the ratio of the Sa_{max} value. The mSIS values are subsequently calculated

using the JMA-SIS program for each scaled ground motion. The final step involved formulating the relationship between mSIS and RS (denoted as rs_mSIS). Validation of the rs_mSIS formulation is then performed to assess its accuracy by comparing it with the results from the JMA-SIS program calculations.

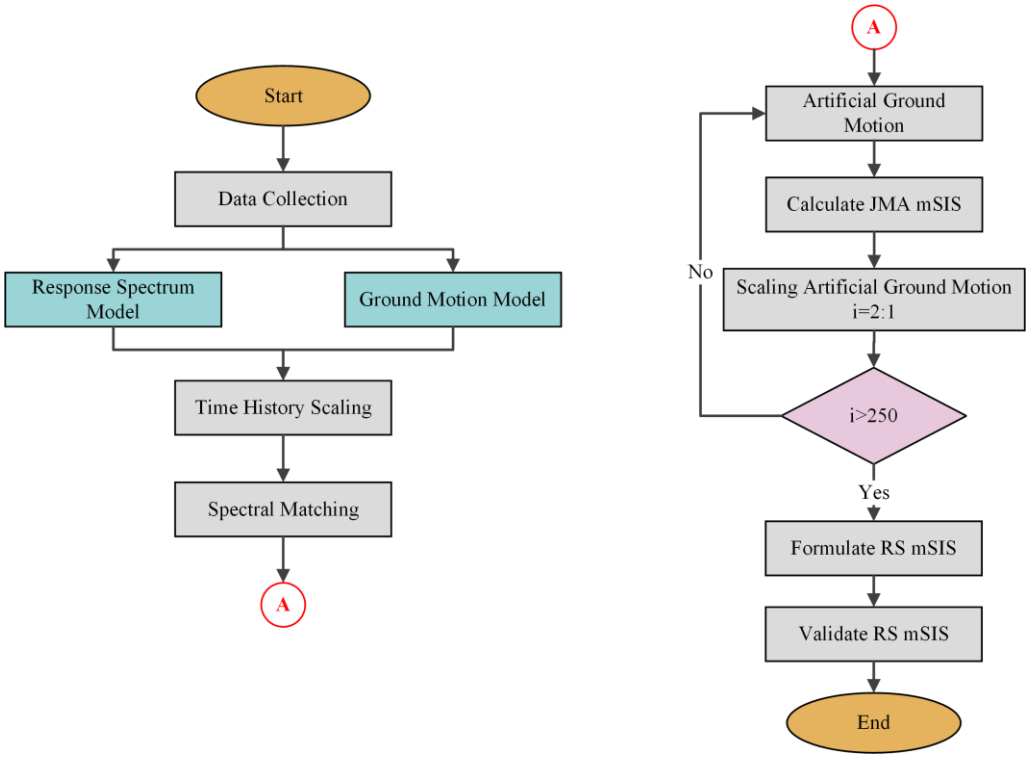

Fig. 4 Research flow chart

2.1. *Formulation of mSIS*

The complete mSIS formulation flow diagram is shown in Fig. 5. The process uses a standard tool for calculating shaking intensity based on JMA-SIS, developed in Matlab (MatlabJMA-SIS). It takes three components of earthquake ground motion—NS, EW, and UD—as input. To begin, the fast Fourier transform (FFT) is applied to each acceleration component, converting the time-domain signals into the frequency domain. Next, the bandpass filters, as defined in Eqs. (1)-(5), are applied to the frequency-domain accelerations:

$$\lambda_1 = \sqrt{\frac{1}{f}} \tag{1}$$

$$\lambda_2 = \frac{1}{\sqrt{1+0.694y^2+0.241y^4+0.0557y^6+0.009664y^8+0.00134y^{10}+0.000155y^{12}}} \tag{2}$$

$$\lambda_3 = \sqrt{1-exp\left(\frac{-f}{0.5}\right)^3} \tag{3}$$

$$y = \frac{f}{10} \tag{4}$$

$$\lambda = \lambda_1 \times \lambda_2 \times \lambda_3 \tag{5}$$

where f denotes the dominant frequency, λ_1 refers to the filter's on-period effect, λ_2 refers to the high-cut filter, and λ_3 refers to the low-cut filter.

After filtering, the accelerations are transformed back from the frequency domain to the time domain. The normalized vector composition of the three acceleration components is then used to calculate the acceleration amplitude. Next, the intensity is automatically calculated from the filtered three-component ground acceleration data, following the application of the bandpass filter. Finally, using the filtered time-domain acceleration and its vectored components, the *mSIS* value is determined using

$$mSIS = 2log(a_{0.3}) + 0.94 \quad (6)$$

where a_{03} represents the minimum peak acceleration sustained over a continuous 0.3-second duration around the maximum acceleration response.

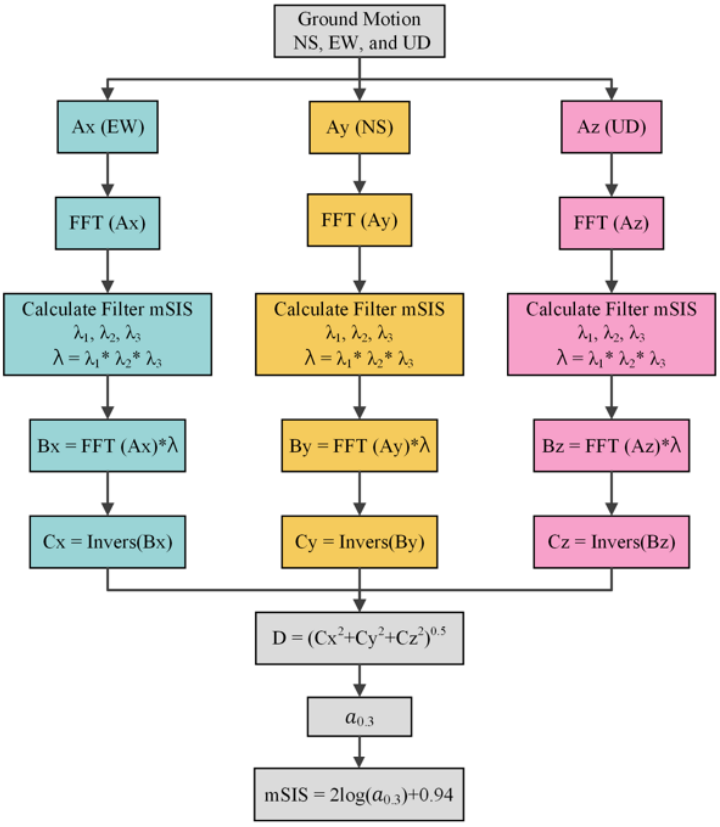

Fig. 5 Flowchart of *mSIS* formulation

2.2. *Calculation of $a_{0.3}$*

The $a_{0.3}$ value is derived from research conducted in the Hongo District of Tokyo between 1894 and 1924. The results indicated that houses and trees are affected only by shaking after the earthquake had lasted for 0.3 seconds [21]. This finding showed that these objects did not experience significant shaking when the acceleration duration is below 0.3 seconds. Therefore, the 0.3-second threshold is confirmed as a key parameter in the mSIS calculation. In this study, the $a_{0.3}$ value was obtained from the three-directional acceleration response: NS, EW, and UD [22]. The graphical representation of the relationship between time and resultant acceleration is shown in Fig. 6(a), while Fig. 6(b) illustrates the cumulative time accumulation method used to calculate the $a_{0.3}$ value. The graph is generated by sorting the acceleration values from highest to lowest, and $a_{0.3}$ is then compared with 0.3/Δt + 1.

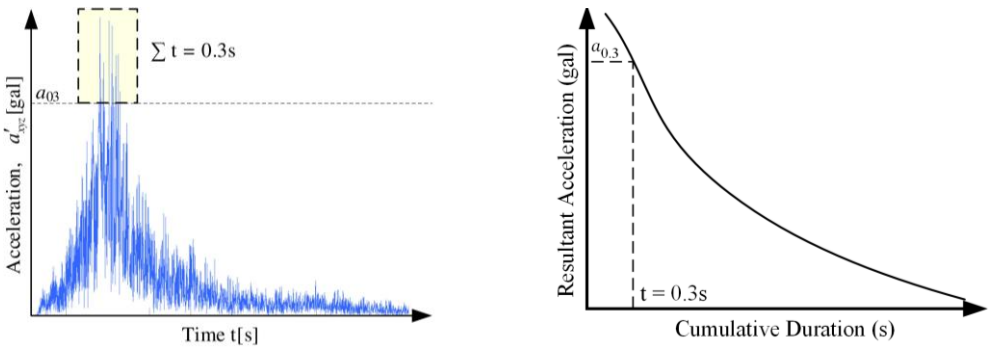

(a) Absolute acceleration graph (b) Determination of $a_{0.3}$ based on cumulative duration [23]

Fig. 6 Calculation of $a_{0.3}$

2.3. Validation of mSIS formulation

Ground motion data and actual mSIS values were obtained from the K-Net website and used for validation [3]. The mSIS values covered all JMA-SIS levels at 0.1 intervals, the calculations performed using the MatlabJMA-SIS tool for the ground motion data are then compared with the actual mSIS values. The comparison between the MatlabJMA-SIS calculations and the K-Net data showed highly accurate results, as the generated equation closely followed the form x≈y with an R^2 value approaching 1. The recorded discrepancy is primarily due to actual mSIS data being rounded to one decimal place, whereas the MatlabJMA-SIS calculations are carried out to three decimal places. These findings demonstrate that the JMA-SIS program effectively validated the mSIS calculations, as shown in the sample data presented in Fig. 7.

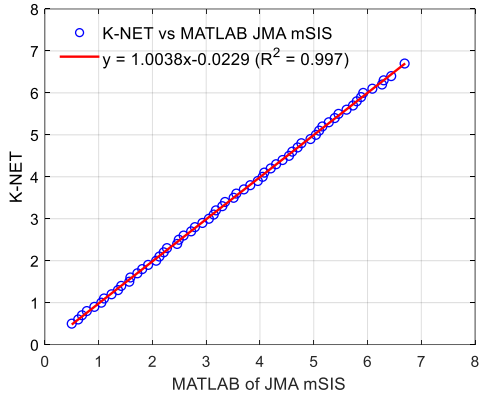

Fig. 7 Comparison of MatlabJMA-SIS vs K-Net

2.4. Response spectrum (*RS*)

The RS used in this research consisted of two components: the 'RS model' and 'RS validation'. The RS model varies based on *Ts* values, ranging from 0.2 to 1.2 seconds in 0.1-second intervals, as shown in Fig. 8. The Sa_{max} value for all *Ts* variations is set to 0.01 g, which is necessary to establish the relationship between RS and mSIS (rs_mSIS). This relationship is achieved by scaling the RS using a factor corresponding to the Sa_{max} value.

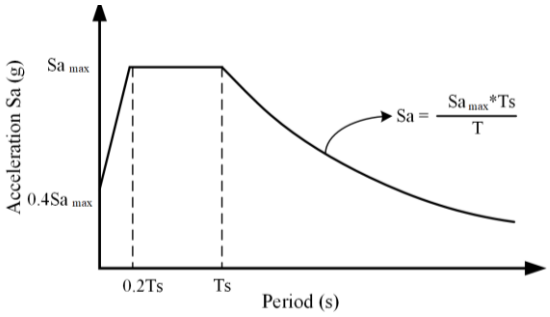

Fig. 8 Response spectrum model

Fig. 9 Distribution map of RS validation data

For RS validation, city samples from the five largest islands in Indonesia are selected, with three cities chosen from each island, totaling 15 RS validation samples. The RS values are obtained following the SNI 1726:2019 guidelines for the earthquake-resistant design of buildings and non-building structures [23]. The validation considered three soil classes: stiff (SC), medium (SD), and soft soil (SE). The distribution map of the selected cities is presented in Fig. 9, while Table 2 presents the corresponding RS validation variables, including T_0 and S_1, for each city.

Table 2 RS validation variables

No.	Island	City	Soil class	Variable of response spectrum			
				T_0	T_s	Sa_{max}	S_1
1	Sumatera	Medan	SC	0.130	0.670	0.810	0.540
		Palembang	SD	0.230	1.130	0.465	0.525
		Padang	SE	0.210	1.050	1.125	1.185
2	Java	Jakarta	SC	0.120	0.600	0.945	0.570
		Surabaya	SD	0.140	0.720	0.855	0.615
		Yogyakarta	SE	0.200	0.990	1.125	1.110
3	Kalimantan	Pontianak	SC	0.070	0.330	0.225	0.075
		Samarinda	SD	0.230	1.150	0.195	0.225
		Palangkaraya	SE	0.280	1.380	0.120	0.165
4	Sulawesi	Manado	SC	0.110	0.550	1.245	0.690
		Makassar	SD	0.140	0.710	0.360	0.255
		Palu	SE	0.200	1.000	1.200	1.200
5	Papua	Sorong	SC	0.100	0.480	1.920	0.915
		Jayapura	SD	0.140	0.700	1.500	1.050
		Nabire	SE	0.200	1.000	1.200	1.200

2.5. Ground motion

The ground motion data used in this study are divided into two categories: model data and validation data. The criteria for the model data are selected based on earthquake source types, magnitude, depth, and epicenter distance, to ensure a comprehensive representation of various earthquake conditions [24]. In contrast, the validation data are selected based on Indonesia's earthquake de-aggregation map [25], following standard ground motion selection procedures. The details of both the models and validation datasets are presented in Table 3 and Table 4, respectively.

Table 3 Ground motion model [26-28]

No.	Earthquake sources	Earthquake	Date	Station	Magnitude (M)	Depth (km)	Epicenter distance (km)
1	Interface Subduction (Megathrust)	Tohoku	11-Mar-2011	Tachikawa	9.00	24.0	256.00
2		Tokachi-Oki	26-Sep-2003	Ikeda	8.00	42.0	138.00
3		Valparaiso	3-Mar-1985	Santiago	8.80	33.0	122.00
4	Deep Subduction (Benioff)	Michoacan	22-May-1997	La Union	6.60	70.0	107.00
5		Hokkaido	25-Feb-2023	Shibetsu	6.00	63.0	101.00
6		Geiyo	24-Mar-2001	Toyo	6.40	51.0	41.00
7	Shallow Crustal / Background	Imperial Valley-02	18-May-1940	El Centro	6.95	8.8	13.00
8		Mammoth Lakes-11	7-Jan-1983	Convict Creek	5.31	4.5	9.70
9		Kozani	19-May-1995	Karpero	5.10	6.8	11.85
10		Umbria	26-Sep-1997	Castelnuovo-Assisi	6.00	10.0	19.90
11		San Francisco	9-Feb-1971	Castaic	6.61	13.0	25.36
12		Taiwan Smart 1	21-Sep-1983	SMART1 I01	6.50	18.0	99.31

Table 4 Ground motion validation [27-29]

No.	Island	City	Ground motion (Earthquake)		
			Megathrust	Benioff	Shallow crustal/ Background
1	Sumatera	Medan	El Pedragal (Chile, 2015.09.16)	Caleta de Campos (Michoacan, 1997.05.22)	Tracy (Livermore01, 1980.01.24)
		Padang	Concepcion San Pedro (Chile, 2010.02.27)	San Miguel (El Salvado, 2001.01.13)	Mission Creek Fault (Landers, 1992.06.28)
		Palembang	Municip (Chile, 2010.02.27)	Santa Ana (El Salvador, 2001.01.13)	Tracy (Livermore01, 1980.01.24)
2	Jawa	Jakarta	CURICO (Chile, 2010.02.27)	Santa Ana (El Salvador, 2001.01.13)	Desert Hot Springs (BigBear-01, 1992.06.28)
		Yogyakarta	Concepcion San Pedro (Chile, 2010.02.27)	Santa Ana (El Salvador, 2001.01.13)	Tolmezzo (Friuli, 1976.05.06)
		Surabaya	Valdivia (Chile, 2010.02.27)	Santa Ana (El Salvador, 2001.01.13)	Mission Creek Fault (Landers, 1992.06.28)
3	Kalimantan	Pontianak	Valdivia (Chile, 2010.02.27)	Caleta De Campos (Michoacan, 1997.05.22)	Kavala (Drama, 1985.11.09)
		Palangkaraya	Daracena (Chile, 2015.09.16)	Santa Ana (El Salvador, 2001.01.13)	LB - City Hall (Northridge-01, 1994.01.17)
		Samarinda	Daracena (Chile, 2015.09.16)	Caleta De Campos (Michoacan, 1997.05.22)	Kavala (Drama, 1985.11.09)
4	Sulawesi	Manado	Narita (Honshu, 2011.03.11)	Santa Ana (El Salvador, 2001.01.13)	Desert Hot Springs (BigBear-01, 1992.06.28)
		Palu	El Pedragal (Chile, 2015.09.16)	San Miguel (El Salvador, 2001.01.13)	Tolmezzo (Friuli, 1976.05.06)
		Makassar	Valdivia (Chile, 2010.02.27)	Santa Ana (El Salvador, 2001.01.13)	LB - City Hall (Northridge-01, 1994.01.17)
5	Papua	Sorong	Valdivia (Chile, 2010.02.27)	San Miguel (El Salvador, 2001.01.13)	Tolmezzo (Friuli, 1976.05.06)
		Nabire	Daracena (Chile, 2015.09.16)	San Miguel (El Salvador, 2001.01.13)	Mission Creek Fault (Landers, 1992.06.28)
		Jayapura	Narita (Honshu, 2011.03.11)	San Miguel (El Salvador, 2001.01.13)	Tolmezzo (Friuli, 1976.05.06)

2.6. Spectral matching

To generate artificial ground motions, the time-history spectra are carefully matched against a predefined target RS model, ensuring accuracy and reliability in representing seismic demands. The target RS is designed for periods ranging from 0.2 to 1.2 seconds, with increments of 0.1 seconds based on the spectral acceleration values (*Ts*). A uniform Sa_{max} value of 0.01 g is applied across all target RS variations to standardize the spectral matching process. Using this approach, a total of 15 target ground motions are selected, resulting in 165 pairs of ground motion data for spectral matching. The RS for the lateral directions (NS, EW, and UD) is combined using the square root sum of squares (SRSS) method, creating a resultant spectrum (RS_SRSS) for further analysis.

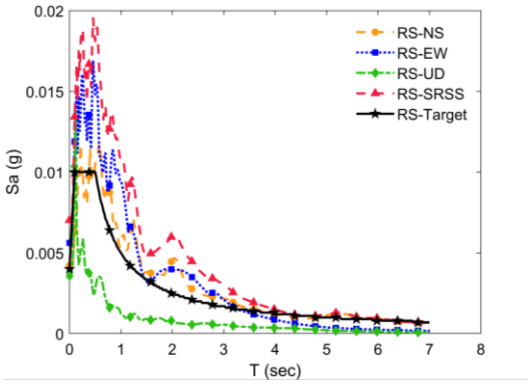

(a) Response spectrum

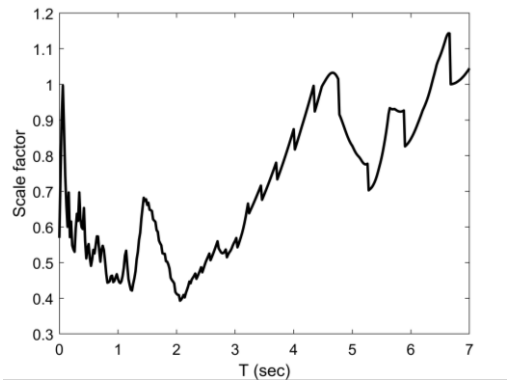

(b) Spectrum scaling

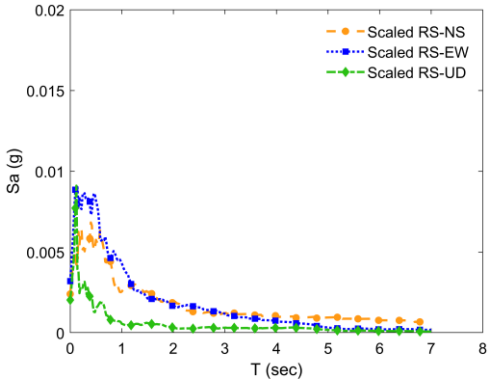

(c) Scaled response spectrum

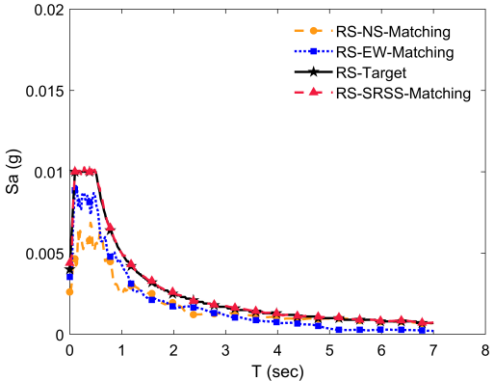

(d) Outcome of spectral matching

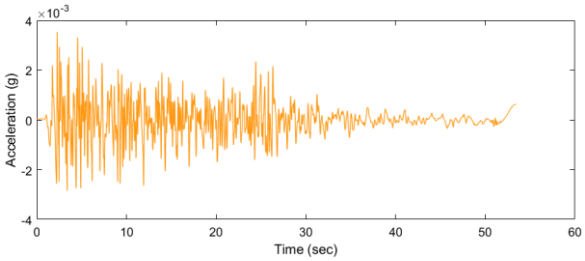

(e) Artificial time history EW

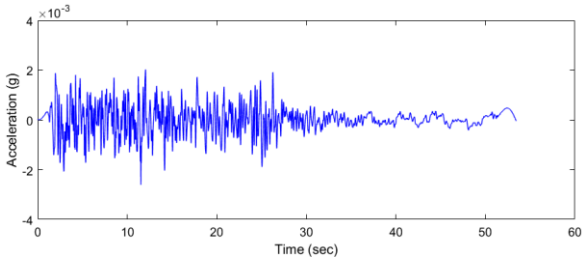

(f) Artificial time history NS

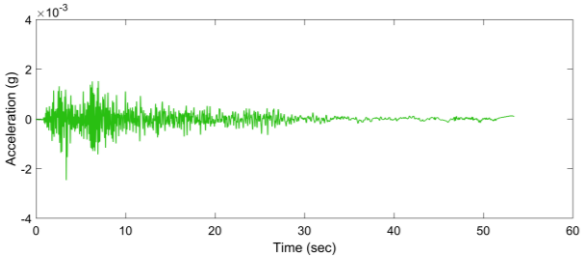

(g) Artificial time history UD

Fig. 10 Spectral matching El Centro earthquake

Fig. 10 illustrates the process of spectral matching using the El Centro earthquake (ELC) time history as an example. In Fig. 10(a), the individual response spectra for the NS, EW, and UD components are shown alongside the RS_Target and the resultant RS_SRSS. This comparison highlights how the original spectra align with the target response spectrum. In Fig. 10(b), the scale factor is depicted, which is calculated as the ratio of RS_Target to RS_SRSS for each specified period. This scale factor serves as a crucial parameter for adjusting the amplitude of the original spectra. Fig. 10(c) presents the scaled response spectrum, obtained by multiplying the original RS by the calculated scale factor. This step ensures that the modified spectrum aligns closely with the RS_Target. Fig. 10(d) showcases the outcome of the spectral matching process, where the matched time-history spectrum is observed to reproduce the target spectrum's shape and amplitude accurately. Finally, Figs. 10(e)-(g) provides a detailed view of the generated artificial ground motions for the NS, EW, and UD directions.

These plots reveal the time-history signals after spectral matching, demonstrating adjustments in amplitude and frequency content to meet the target RS requirements. Collectively, these figures illustrate the comprehensive and iterative approach employed in generating artificial ground motions, ensuring consistency with and adherence to the target seismic characteristics.

3. Results and Discussion

A total of 165 pairs of artificial ground motions are generated through spectral matching and used to calculate the mSIS values using the JMA-SIS program. The next step was determining the average mSIS values for each ground motion model, based on variations in the target RS. These variations depend on different Ts values, which represent the period of the seismic event. The results are presented in Table A-2 (Appendix 2). The mSIS values listed in Table 5 correspond to variations of *Ts* in the target RS with a Sa_{max} value of 0.01 g. These values are calculated by applying a scaling factor to the artificial ground motion, with the scaling factor ranging from 1 to 250, corresponding to the Sa_{max} ratio.

3.1. Formulation of rs_mSIS

The relationship between Sa_{max} and mSIS is shown in Fig. 11 to derive an equation relating Sa_{max} to mSIS. It is found that the relationship between Sa_{max} and mSIS follows a logarithmic pattern, with an R^2 value of 1, indicating a strong correlation. This suggests that Sa_{max} is a reliable predictor of mSIS values across different seismic conditions. All variations of the RS produced the same pattern, leading to the formulation below

$$mSIS = 2\log(Sa_{\max}) + A \tag{7}$$

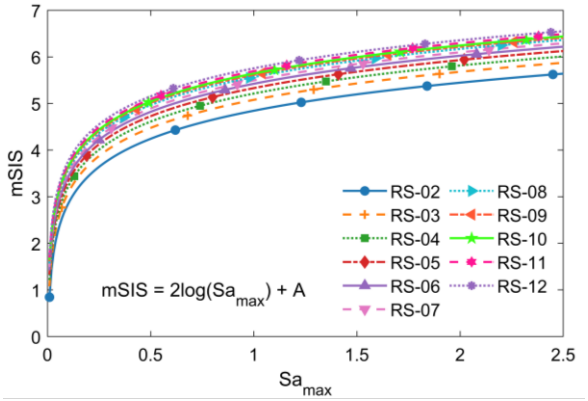

Fig. 11 Relationship between Sa_{max} and mSIS

Eq. (7) is derived by formulating the mSIS values calculated based on the RS variable and is referred to as 'rs_mSIS'. It is observed that this equation closely resembled the general mSIS formulation in Eq. (6), indicating a strong relationship between the Samax variables and $a_{0.3}$. The rs_mSIS equation exhibits the same pattern across all variations of RS, with the only difference being the coefficient *A*, which leads to the formulation of the relationship between the *Ts* value and coefficient *A*. The *W* values are in accordance with the values presented in Table 5.

Table 5 Coefficient *A* and *W* values

Response spectrum	Ts (sec)	Ts - 0.7 (sec)	Coefficient A	W = (A - 5.496)
RS_02	0.2	-0.5	4.856	-0.638
RS_03	0.3	-0.4	5.095	-0.399
RS_04	0.4	-0.3	5.222	-0.272
RS_05	0.5	-0.2	5.338	-0.156
RS_06	0.6	-0.1	5.418	-0.077
RS_07	0.7	0.0	5.495	0.000
RS_08	0.8	0.1	5.578	0.084
RS_09	0.9	0.2	5.609	0.115
RS_10	1.0	0.3	5.646	0.151
RS_11	1.1	0.4	5.705	0.211
RS_12	1.2	0.5	5.759	0.264

Meanwhile, the normalization of RS_07 is required to establish the Ts-A relationship, as detailed in Table 5. It is later found that the graph depicting the relationship between the (Ts–0.7) value and coefficient *W* followed a quadratic equation with an R^2 value of 0.990, as shown in Fig. 12. This strong correlation further supports the robustness of the derived equations. Eq. (7), along with the graph of the relationship between (Ts-0.7) and the coefficient *W*, is used to formulate the *rs_mSIS* equation, and can be expressed as

$$rs\_mSIS = 2\log(Sa_{\max}) + 5.495 + W \tag{8}$$

$$W = -0.696(Ts - 0.7)^2 + 0.812(Ts - 0.7) \tag{9}$$

where *rs_mSIS* is *mSIS* based on the response spectrum, Sa_{max} denotes the response spectrum variable (maximum *Sa*), and *W* refers to the Wariyatno coefficient.

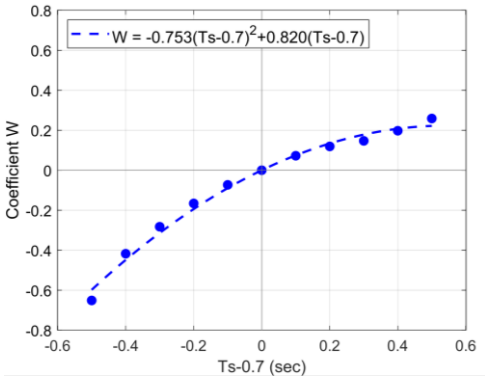

Fig. 12 Relationship between (Ts-0.7) and coefficient *W*

3.2. Relationship between Sa_{max} and $a_{0.3}$

The rs_mSIS formulation required validation to ensure the reliability of the results. To achieve this, validation data are extracted from the actual response spectrum (RS) according to SNI 1726:2019 [24], while ground motion validation data are selected based on Indonesia's earthquake de-aggregation map of. These datasets are used to generate artificial ground motions, and mSIS values are calculated using both the JMA-SIS program and the rs_mSIS equation. The results from the JMA-SIS program and the *rs_mSIS* equation are compared, as shown in Table A-3 (Appendix 3). It is found that the deviation between the two methods is minimal, with an average deviation of 1.024% and a maximum deviation of 2.372%. These findings confirm that the rs_mSIS equation can reliably predict mSIS based on RS. Furthermore, Eq. (10) closely resembles Eq. (6), which is used to establish the relationship between Sa_{max} and $a_{0.3}$ as follows:

$$\frac{a_{0.3}}{Sa_{\max}} = 10^{2.278+\frac{W}{2}} \tag{10}$$

where $a_{0.3}$ is JMA-SIS acceleration vector accumulated over 0.3 seconds, expressed in *Gal* (1 *Gal* = 1 cm/s^2).

3.3. Implementation of quantitative SIS

Fig. 13 illustrates the quantitative determination scheme of the SIS for a residential building. Once the building passes the seismic design phase, the next step is to assess the level of shaking it will experience. The RS selected during the design phase is used to generate the seismic wave for the construction site, taking into account both the soil conditions and the building's dynamic characteristics. A time-history analysis is then performed, using seismic waves as the input ground motion.

The results of the time-history analysis are used to evaluate the accelerations at various floors of the building. The FFT method is applied to these accelerations to identify the dominant period of each floor and the peak response acceleration. These predominant periods and peak accelerations are plotted on the JMA-SIS scale to determine the shaking levels for each floor.

If any floor exceeds the permissible SIS threshold, the building design must be revised to address this issue. The permissible seismic intensity level, which is critical for reducing human casualties during significant earthquakes, should be defined in seismic design codes to ensure safety.

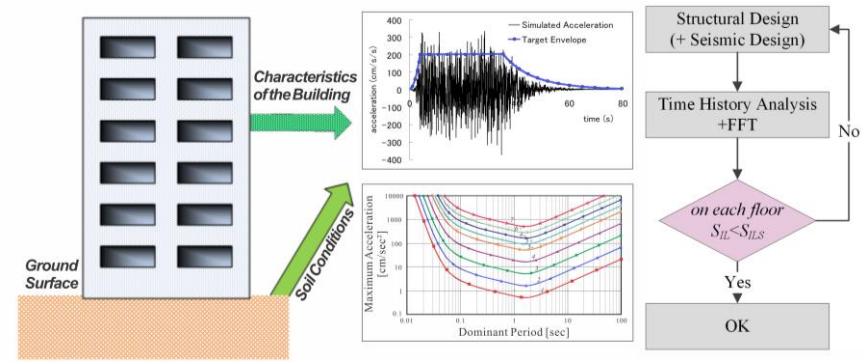

Fig. 13 Quantitative SIS implementation [12]

4. Conclusions

This study presents a novel and reliable approach for calculating earthquake shaking intensity (mSIS) through the response spectrum-based index (rs_mSIS), using the JMA-SIS as a benchmark. By identifying maximum spectral acceleration (Sa_{max}) and the associated period (Ts) as key parameters, the research successfully formulated rs_mSIS as a logarithmic function of Sa_{max}. The strong alignment of this formulation with the JMA-SIS equation confirms its theoretical validity and strengthens the central argument that response spectrum data can be effectively utilized to estimate seismic intensity with high accuracy.

The model's robustness was verified using ground motion data from 15 cities in Indonesia, where the rs_mSIS yielded highly consistent and dependable predictions. A notable contribution of this study is the revealed correlation between $a_{0.3}$ and Sa_{max} under spectrally matched ground motions, emphasizing the sensitivity of the rs_mSIS model to realistic seismic input conditions. These insights contribute to a deeper understanding of ground motion characteristics and their impact on seismic intensity measures.

Beyond methodological advancement, the findings align with the broader objective of strengthening seismic resilience in earthquake-prone regions. By introducing a standardized and accurate tool for estimating ground shaking, the rs_mSIS model facilitates safer structural design, informed urban planning, and improved zoning and building regulations. Ultimately, this study contributes to both technical progress and the societal goal of reducing earthquake risks through science-based preparedness and policy.

5. Future Recommendation

It should be noted that this study does not include specific case studies, which may limit the direct applicability of the model to unique urban environments. While the methodology presented can be applied to cities with varying seismic activity, such as those in Indonesia, as demonstrated by the RS validation data, further case-specific studies are needed to fully assess the model's effectiveness in different regions with varying geotechnical and structural conditions.

Acknowledgments

The authors gratefully acknowledge the financial assistance provided by the Institute for Research and Community Service (LPPM), Universitas Jenderal Soedirman (UNSOED), Indonesia (27.114/UN23.37/PT.01.03/II/2023). This research was also partially supported by Universitas Diponegoro (UNDIP), Indonesia, through the World Class University program (1161/UN7.A4/KU/X/2023).

Conflicts of Interest

The authors declare no conflict of interest.

References

[1] J. Bustos, C. Pastén, D. Pavez, M. Acevedo, S. Ruiz, and R. Astroza, "Two-Dimensional Simulation of the Seismic Response of the Santiago Basin, Chile," Soil Dynamics and Earthquake Engineering, vol. 164, article no. 107569, 2023.

[2] V. Y. Sokolov, "Seismic Intensity and Fourier Acceleration Spectra: Revised Relationship," Earthquake Spectra, vol. 18, no. 1, pp. 161-187, 2002.

[3] National Research Institute for Earth Science and Disaster Resilience, "Strong-Motion Seismograph Networks," https://www.kyoshin.bosai.go.jp/kyoshin/search/index_en.html, accessed on 2023.

[4] S. Li, Y. Chen, and T. Yu, "Comparison of Macroseismic-Intensity Scales by Considering Empirical Observations of Structural Seismic Damage," Earthquake Spectra, vol. 37, no. 1, pp. 449-485, 2021.

[5] L. Serva, E. Vittori, V. Comerci, E. Esposito, L. Guerrieri, A. M. Michetti, et al., "Earthquake Hazard and the Environmental Seismic Intensity (ESI) Scale," Pure and Applied Geophysics, vol. 173, no. 5, pp. 1479-1515, 2016.

[6] V Sokolov, T Furumura, and F. Wenzel, "On the Use of JMA Intensity in Earthquake Early Warning Systems," Bulletin of Earthquake Engineering, vol. 8, no. 4, pp. 767-786, 2010.

[7] A. Sakai, "Generalization of Calculation Method for Seismic Intensity Using Filtered Acceleration," The International Journal of Engineering and Science, vol. 7, no. 5, pp. 34-51, 2018.

[8] "Tables Explaining the JMA Seismic Intensity Scale," https://www.jma.go.jp/jma/en/Activities/inttable.html, accessed on 2023.

[9] "Seismic Intensity," https://www.jma.go.jp/jma/en/Activities/earthquake.html, accessed on 2023.

[10] A. Sakai, "An Expression of the Seismic Intensity Level for a Long-Period Ground Motion," Journal of Japan Society of Civil Engineers, vol. 3, no. 1, pp. 160-173, 2015.

[11] N. G. Wariyatno, H. A. Lie, F. P. Hsiao, and B. S. Gan, "Design Philosophy for Buildings' Comfort-Level Performance," Advances in Technology Innovation, vol. 6, no. 3, pp. 157-168, 2021.

[12] N. G. Wariyatno, A. L. Han, and B. S. Gan, "Proposed Design Philosophy for Seismic-Resistant Buildings," Civil Engineering Dimension, vol. 21, no. 1, pp. 1-5, 2019.

[13] V. Manfredi, A. Masi, A. G. Özcebe, R. Paolucci, and C. Smerzini, "Selection and Spectral Matching of Recorded Ground Motions for Seismic Fragility Analyses," Bulletin of Earthquake Engineering, vol. 20, pp. 4961-4987, 2022.

[14] N. Girmay, E. Miranda, and A. Poulos, "Orientation and Intensity of Maximum Response Spectral Ordinates During the December 20, 2022 Mw 6.4 Ferndale, California Earthquake," Soil Dynamics and Earthquake Engineering, vol. 176, article no. 108323, 2024.

[15] R.A. Medina, R. Sankaranarayanan, and K. M. Kingston, "Floor Response Spectra for Light Components Mounted on Regular Moment-Resisting Frame Structures," Engineering Structures, vol. 28, no. 14, pp. 1927-1940, 2006.

[16] P. Haldar, Y. Singh, D. H. Lang, and D. K. Paul, "Comparison of Seismic Risk Assessment Based on Macroseismic Intensity and Spectrum Approaches Using 'SeisVARA," Soil Dynamics and Earthquake Engineering, vol. 48, pp. 267-281, 2013.

[17] C. Kumar, S. Chatterjee, T. Oommen, and A. Guha, "New Effective Spectral Matching Measures for Hyperspectral Data Analysis," International Journal of Remote Sensing, vol. 42, no. 11, pp. 4126-4156, 2021.

[18] "Seismosoft," https://seismosoft.com, accessed on 2023.

[19] N. G. Damian, and R. Diaferia, "Assessing Adequacy of Spectrum-Matched Ground Motions for Response History Analysis," Earthquake Engineering & Structural Dynamics, vol. 42, no. 9, pp. 1265-1280, 2013.

[20] R. Zhang, L. Zhang, C. Pan, Q. Chen, and Y. Wang, "Generating High Spectral Consistent Endurance Time Excitations by a Modified Time-Domain Spectral Matching Method," Soil Dynamics and Earthquake Engineering, vol. 145, article no. 106708, 2021.

[21] M. Ishimoto, "Echelle d'intensite Seismique et Acceleration Maxima," Bulletin of the Earthquake Research Institute, vol. X, no. 3, pp. 614-626, 1932.

[22] E. Nouchi, N. G. Wariyatno, A. L. Han, and B. S. Gan, "Comfort-Based Criteria for Evaluating Seismic Strengthening Performance of Building," IOP Conference Series: Earth and Environmental Science, vol. 1195, article no. 012002, 2023.

[23] Guidelines for Earthquake-Resistant Design of Building and Non-Building Structures, Indonesian National Standard 1726, 2019.

[24] E. Saputra and L. Makrup, “Deagregasi Hazard dan Rekomendasi Ground Motion Sintetik di Provinsi Riau,” Agregat, vol. 6, no. 1, pp. 505-510, 2021.
[25] Indonesian Earthquake Hazard Deaggregation Maps for Earthquake-Resistant Infrastructure Design and Evaluation, Jakarta, Indonesia: Ministry of Public Works and Public Housing, 2022.
[26] “Strong-Motion Seismograph Networks,” https://www.kyoshin.bosai.go.jp/, accessed on 2023.
[27] “Strong-Motion Virtual Data Center (VDC),” https://www.strongmotioncenter.org/vdc/scripts/earthquakes.plx, accessed on 2023.
[28] “PEER Ground Motion Database,” https://ngawest2.berkeley.edu/spectras/661775/searches/615283/edit, accessed on 2023.
[29] “Center for Engineering Strong Motion Data,” https://www.strongmotioncenter.org/, accessed on 2023.

Appendix 1

Fig. A-1 Illustration of events during an earthquake based on JMA-SIS [9]

Appendix 2

Table A-2 Calculation results of mSIS based on the ground motion model

No.	Ground Motion	JMA-SIS										
		RS-02-01	RS-03-01	RS-04-01	RS-05-01	RS-06-01	RS-07-01	RS-08-01	RS-09-01	RS-10-01	RS-11-01	RS-12-01
1.	TAC	0.785	1.100	1.242	1.334	1.396	1.392	1.490	1.536	1.613	1.616	1.633
2.	IKE	0.850	1.058	1.211	1.334	1.441	1.487	1.653	1.589	1.638	1.639	1.800
3.	SAN	0.871	1.093	1.227	1.382	1.356	1.495	1.535	1.597	1.604	1.722	1.814
4.	LAU	0.861	1.026	1.148	1.283	1.341	1.441	1.609	1.698	1.619	1.596	1.720
5.	SHI	0.928	1.208	1.249	1.378	1.499	1.606	1.605	1.643	1.736	1.786	1.772
6.	TOY	0.825	1.077	1.303	1.271	1.369	1.440	1.514	1.558	1.627	1.717	1.694
7.	ELC	0.944	1.146	1.201	1.288	1.378	1.493	1.548	1.618	1.578	1.713	1.689
8.	CON-V	0.859	1.080	1.215	1.402	1.507	1.603	1.757	1.718	1.546	1.918	1.992
9.	KAR	0.888	1.115	1.221	1.349	1.492	1.512	1.680	1.635	1.798	1.680	1.685
10.	CAS-A	0.864	1.100	1.166	1.262	1.294	1.412	1.392	1.535	1.479	1.539	1.581
11.	CAS	0.849	1.085	1.238	1.414	1.550	1.612	1.713	1.705	1.871	1.863	1.857
12.	SMA	0.752	1.053	1.245	1.362	1.390	1.443	1.442	1.483	1.640	1.676	1.869
	Average	**0.856**	**1.024**	**1.222**	**1.338**	**1.418**	**1.495**	**1.578**	**1.609**	**1.646**	**1.705**	**1.759**

Note: The naming convention for the response spectrum is *RS-Ts-*Sa_{max}. RS 02: Response Spectrum with *Ts* = 0.2 sec

Appendix 3

Table A-3 Validation Results of rs_mSIS Equation

Island	City	Soil Type	Variable of RS		JMA_mSIS				rs_mSIS	Deviasi (%)
			Ts	Sa_{max}	Megathrust	Benioff	Shallow Crustal /Background	Average		
Sumatera	Medan	SC	0.67	0.810	5.237	5.307	5.147	5.231	5.287	1.078%
	Padang	SE	1.05	1.125	5.760	5.585	5.862	5.736	5.796	1.057%
	Palembang	SD	1.13	0.465	4.945	5.017	4.903	4.955	5.050	1.931%
Jawa	Jakarta	SC	0.60	0.945	5.254	5.293	5.387	5.311	5.358	0.876%
	Yogyakarta	SE	0.99	1.125	5.728	5.545	5.648	5.640	5.774	**2.372%**
	Surabaya	SD	0.72	0.855	5.303	5.404	5.358	5.355	5.375	0.372%
Kalimantan	Pontianak	SC	0.33	0.225	3.806	3.760	3.818	3.795	3.804	0.237%
	Palangkaraya	SE	1.38	0.120	3.905	3.944	3.841	3.897	3.884	0.329%
	Samarinda	SD	1.15	0.195	4.198	4.232	4.318	4.249	4.300	1.180%
Sulawesi	Manado	SC	0.55	1.245	5.550	5.513	5.574	5.546	5.548	0.034%
	Palu	SE	1.00	1.200	5.704	5.705	5.723	5.711	5.834	2.168%
	Makasar	SD	0.71	0.360	4.576	4.696	4.529	4.600	4.616	0.335%
Papua	Sorong	SC	0.48	1.920	5.823	5.914	5.726	5.821	5.849	0.487%
	Nabire	SE	1.00	1.200	5.671	5.790	5.737	5.733	5.834	1.770%
	Jayapura	SD	0.70	1.500	5.799	5.786	5.758	5.781	5.847	1.140%
									Average	**1.024%**
									Maximum	**2.372%**